



HAL
open science

Energy analysis of two-phase secondary refrigeration in steady-state operation, Part 1: global optimization and leading parameter

Michel Pons, Hong-Minh Hoang, Thomas Dufour, Laurence Fournaison,
Anthony Delahaye

► To cite this version:

Michel Pons, Hong-Minh Hoang, Thomas Dufour, Laurence Fournaison, Anthony Delahaye. Energy analysis of two-phase secondary refrigeration in steady-state operation, Part 1: global optimization and leading parameter. *Energy*, 2018, 161, pp.1282-1290. 10.1016/j.energy.2018.07.055 . hal-01843005

HAL Id: hal-01843005

<https://hal.science/hal-01843005>

Submitted on 18 Jul 2018

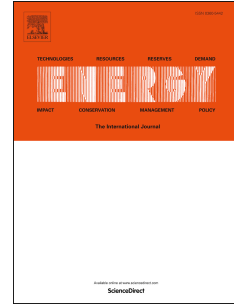
HAL is a multi-disciplinary open access archive for the deposit and dissemination of scientific research documents, whether they are published or not. The documents may come from teaching and research institutions in France or abroad, or from public or private research centers.

L'archive ouverte pluridisciplinaire **HAL**, est destinée au dépôt et à la diffusion de documents scientifiques de niveau recherche, publiés ou non, émanant des établissements d'enseignement et de recherche français ou étrangers, des laboratoires publics ou privés.

Accepted Manuscript

Energy analysis of two-phase secondary refrigeration in steady-state operation, part 1: Global optimization and leading parameter

Michel Pons, Hong-Minh Hoang, Thomas Dufour, Laurence Fournaison, Anthony Delahaye



PII: S0360-5442(18)31352-5

DOI: [10.1016/j.energy.2018.07.055](https://doi.org/10.1016/j.energy.2018.07.055)

Reference: EGY 13320

To appear in: *Energy*

Received Date: 11 February 2018

Revised Date: 6 July 2018

Accepted Date: 9 July 2018

Please cite this article as: Pons M, Hoang H-M, Dufour T, Fournaison L, Delahaye A, Energy analysis of two-phase secondary refrigeration in steady-state operation, part 1: Global optimization and leading parameter, *Energy* (2018), doi: 10.1016/j.energy.2018.07.055.

This is a PDF file of an unedited manuscript that has been accepted for publication. As a service to our customers we are providing this early version of the manuscript. The manuscript will undergo copyediting, typesetting, and review of the resulting proof before it is published in its final form. Please note that during the production process errors may be discovered which could affect the content, and all legal disclaimers that apply to the journal pertain.

Energy analysis of two-phase secondary refrigeration in steady-state operation,

Part 1: global optimization and leading parameter

Michel Pons^{1*}, Hong-Minh Hoang², Thomas Dufour^{1,2}, Laurence Fournaison²,

Anthony Delahaye²

1 LIMSI, CNRS, Université Paris-Saclay, Rue J. von Neumann bât 508, 91405 Orsay Cedex, France

2 Irstea, GPAN ENERFRI, 1 Rue Pierre-Gilles de Gennes, CS 10030, 92261 Antony Cedex, France

* Corresponding author: Michel.pons@limsi.fr

Abstract

A great deal of attention is paid to secondary refrigeration as a means of reducing excessively high emissions of refrigerants (most of which have a potent greenhouse effect) due to leaks in large cooling units. Among the environmentally friendly fluids that can be used in secondary circuits for transporting and storing cold, hydrate slurries offer the advantage of significant latent heats of fusion associated with good fluidity. Research programs have focused attention on hydrate systems, including CO₂, TBPB (tetra-n-butyl-phosphonium-bromide), and mixed CO₂-TBPB hydrates. In addition to feasibility concerns, energy efficiency is also a crucial concern requiring an objective analysis of the improvements likely to result from these new materials. An impartial framework was thus constructed based on the principles of optimization methods. This approach was applied to these three hydrate slurries as well as to the well-known ice slurry for comparison purposes. A numerical model of secondary

refrigeration system in steady state was built, on the basis of which optimized systems subjected to common external constraints can be designed for each slurry according to its thermophysical properties. Global performance can then be compared on a sound basis, which also makes it possible to identify the hydrate property that is most influential on energetic performance. Part 2 of this study is dedicated to exergy analysis and phase change kinetics.

Keywords

Refrigeration, phase change material, hydrate, slurry, process optimization, CO₂, TBPB, ice.

Nomenclature

Usual notations (T for temperature, P for pressure, \dot{Q} for heat fluxes, Re for Reynolds number, etc.) are not recalled here.

A heat-transfer area [m^2]

COP Coefficient Of Performance of the primary cooling unit

D hydraulic diameter [m]

f Fanning friction factor [-].

L distance between the primary cooling unit and the end-user [m]

K, n rheology parameter for non-Newtonian fluids

u flow velocity [$\text{m}\cdot\text{s}^{-1}$]

U overall heat transfer coefficient [$\text{W}\cdot\text{m}^{-2}\cdot\text{K}^{-1}$]

x additive concentration in its aqueous solution [$\text{kg}\cdot\text{kg}^{-1}$]

X solid mass fraction in the slurry [$\text{kg}\cdot\text{kg}^{-1}$]

y axial position [m]

Y component fraction in the solid phase [$\text{kg}\cdot\text{kg}^{-1}$]

Greek symbols

χ mass fraction in the total flow [$\text{kg}\cdot\text{kg}^{-1}$]

ϕ crystal volume fraction in the slurry [$\text{m}^3\cdot\text{m}^{-3}$]

η efficiency (isentropic) [-]

σ carbon dioxide solubility in aqueous phase [$\text{kg}\cdot\text{kg}^{-1}$]

Indexes

0 initial liquid solution ($W + A$)

1-7 refer to points in Fig. 1

A additive

C condenser

CD carbon dioxide

E evaporator

eq equilibrium

f fusion

G gas phase

$HX\bullet$ referred to the corresponding heat exchanger, C , E or U .

I insulation

in inlet of a HX section

L liquid phase

P slurry pump

PC primary compressor

S solid phase (crystals)

T total

U user

W Water (H_2O)

1 Introduction

One of the challenges facing the refrigeration industry is the need for drastic reduction of its contribution to global warming. The Global Warming Potential (GWP) of current refrigerant fluids is on the order of several thousand [1, 2], yet large cooling units unfortunately experience significant leakage rates. After adding in the indirect effects due to energy consumption, this industry contributes as much as 8% of all greenhouse gas emissions. Research on new refrigerants with low GWP is underway, but secondary refrigeration is an already existing solution: when distributing cold via a loop containing an environmentally friendly fluid, the volume of refrigerant as well as leaks can be severely limited. Until recently, the choice of a secondary fluid was essentially limited to chilled water and ice slurry. Chilled water transports sensible heat, which requires significant flow rates, while the latent heat transported by ice slurries is delivered at temperatures below 0°C. However, a new class of phase-change materials is emerging for refrigeration applications: hydrate slurries. Well-known in the petroleum industry, semi-clathrate hydrates are ice-like crystals where H₂O molecules form cages around host molecules. These molecules can be a gas (CH₄, CO₂, alkanes, SO₂, etc.) or salts like tetra-n-butyl-ammonium-, or phosphonium-bromide (respectively TBAB and TBPB). *Mixed* hydrates may also form, e.g. with CO₂-TBPB [3]. These two-phase solid-liquid materials offer several advantages: the transport of latent heat [4, 5], good fluidity [6], and such a wide variety that the phase-change temperature can be adapted to the design application [7]. Hydrate slurries are thus good options for secondary refrigeration [8-10] or cold storage [7, 11]. Their rheology [12, 13], thermal properties [14, 15], and phase-change kinetics [11, 16, 17] have been studied extensively. Apart from these characterization studies, performance analyses of secondary refrigeration systems using hydrate slurries are still scarce [18-21]. They may invoke various features as efficiency

arguments, including significant latent heat of fusion, fusion temperature, low viscosity, rapid kinetics, etc. This makes it difficult to compare the various slurries on common criteria.

The purpose of this article is to build a thermodynamic framework for evaluating the energy efficiency of secondary fluids and comparing them on a sound and impartial basis. The approach adopts the fundamental principle of optimization, i.e. minimization of an objective function under given constraints equally applied to each system under comparison. Four slurries were considered, three with either CO₂-hydrate, TBPB-hydrate, or CO₂-TBPB mixed hydrate, as well as the ice slurry for comparison purposes. These four slurries were chosen for their variety of thermodynamic properties, enthalpy of fusion, viscosity and rheological behavior, melting temperature, and presence or absence of gaseous CO₂. Rather than simply ranking these slurries, one purpose of this study is to ascertain which slurry property has the leading influence on energy efficiency by using thermodynamics-based arguments. A numerical model of secondary refrigeration system in steady-state was built. For each of the four slurries, this model was used for designing the system that minimizes the energy consumption and fulfills the prescribed constraints. The four systems can then be compared on a fair basis.

2 Thermodynamic framework

In thermodynamic terms, a secondary refrigeration loop simply transports heat from the *user*, e.g. an air-conditioned room or food needing to be preserved, to the *primary cooling* unit, or more precisely to its evaporator. The loop itself is merely a dissipative process, while the primary unit converts electricity into cold production. As the notion of energy efficiency only makes sense for energy conversion processes, energy analysis of secondary refrigeration can be relevant only when it considers the whole system, secondary loop plus primary unit, as presented in Fig. 1. This framework contains all the basic components of secondary refrigeration. The loop (123451) transports cold to the user over the distance L . Ice- or

hydrate-crystals are generated in the *HXE* heat exchanger, which also is the evaporator of the cooling unit. The slurry circulates in the loop via the pump *P* and receives the heat flux \dot{Q}_I from ambient air through the thermal insulation of the secondary circuit. Most of these crystals melt in the user's heat exchanger *HXU*. The cooling unit consumes mechanical power for its primary compressor (*PC*) and rejects heat outdoors through its condenser (*HXC*). When the hydrate contains CO_2 , crystal fusion produces gaseous CO_2 . This gas is separated from the slurry at the outlet of *HXU*; it is re-pressurized in the gas-compressor *C_G* and circulated via the line (67) toward the *HXE*, where it contributes to formation of new hydrates.

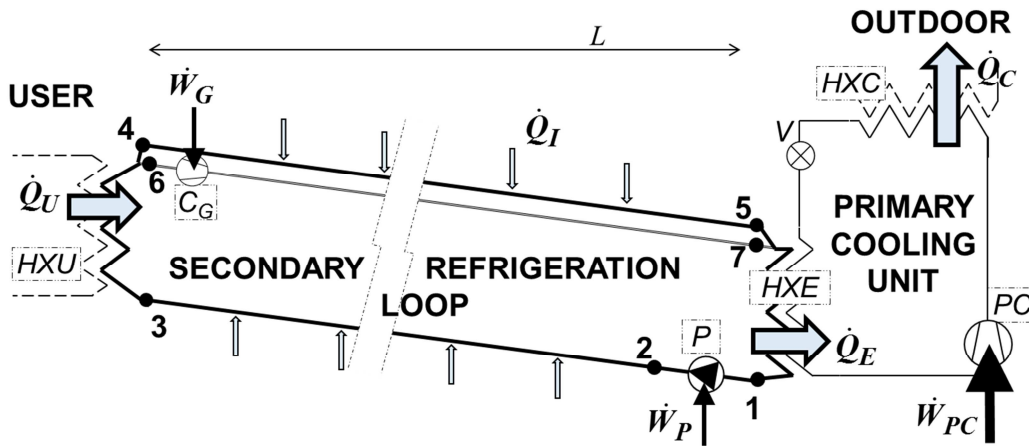


Fig. 1: Sketch of a secondary refrigeration process. 123451: slurry loop; *P*: slurry circulation-pump; *HXU*, *HXE* and *HXC*: heat exchangers on the user's side, at the evaporator and at the condenser of the primary cooling unit, respectively; *PC*: primary compressor; *V*: throttling valve; 67: return line for gaseous CO_2 and *C_G*: gas compressor (when involved). L = distance between user and primary cooling unit.

When applied to this global system, the First Law in steady state gives the following balances:

$$\dot{Q}_E = \dot{Q}_U + \dot{Q}_I + \dot{W}_P + \dot{W}_G \quad (1)$$

$$\dot{Q}_C = \dot{Q}_E + \dot{W}_{PC} = \dot{Q}_E \cdot (1 + COP^{-1}) \quad (2)$$

The *COP* of the primary cooling unit (\dot{Q}_E / \dot{W}_{PC}) is related to the internal exergy efficiency of the primary cycle η_{PC} (accounting for non-isentropic compression and expansion) by:

$COP = \eta_{PC} \cdot T_E / (T_C - T_E)$. The total consumption of mechanical energy is $\dot{W}_T = \dot{W}_{PC} + \dot{W}_P + \dot{W}_G$; among these three terms \dot{W}_{PC} is expected to be largely dominant, while the other two should only represent a small percentage of \dot{Q}_U .

3 Principle of process optimization

Essentially, optimization consists designing various configurations for a given purpose and with prescribed *constraints*, and then selecting the configuration that minimizes a given criterion called *cost function*. Constraints are an important facet of optimization, although rarely explicit. Applying the same constraints to any configuration under consideration makes each designed configuration independent and self-consistent, so that the configuration that minimizes the cost function is truly optimum.

Globally, the process consists of extracting the heat flux \dot{Q}_U from the user while consuming the total mechanical energy \dot{W}_T , and the main concern is energy efficiency. Prescribing the *duty* of the process, i.e. the heat flux \dot{Q}_U ($\dot{Q}_U = 30\text{kW}$) forms constraint #1. The cost function to minimize herein is then exactly represented by \dot{W}_T . The next constraints are economic ones: investment costs must be roughly the same for all cases. As the total investment cost is impacted primarily by the size of heat exchangers, this economic condition is reflected as conditions on heat exchange areas. For constraint #2, the area of the heat exchanger *HXE* between evaporation and crystal generation in the slurry is prescribed ($A_{HXE} = 6\text{m}^2$). Constraint #3 is that the total area of the two heat exchangers, *HXU* and *HXC*, is given ($A_{HXU} + A_{HXC} = 35\text{m}^2$). Indeed, both heat exchangers involve a forced flow of air and have similar technologies. Moreover, the *HXU* area depends on the crystal fusion temperature. Constraint #3 allows for redistributing the total area between the two heat exchangers in the same way a designer would do.

The last constraint is a technical one: it is important to prevent the slurry flow from being blocked by sedimentation and aggregation of crystal particles anywhere in the secondary circuit. This can be done by forcing the slurry flow to be turbulent. For non-Newtonian pseudoplastic fluids, turbulence is fully developed for Reynolds numbers above 4000. This value is thus imposed as a minimum for the Reynolds number almost everywhere (constraint #4). Indeed, the heat flux from the user makes this condition less crucial in the *HXU* heat exchanger, where the minimal Reynolds value can thus be lowered to 2500, a value that still lies within the laminar-turbulent transition domain. An a posteriori check was performed to ensure that the slurry velocity always lies above $0.5\text{m}\cdot\text{s}^{-1}$, another condition for preventing blockage according to [22].

Several other design parameters are also prescribed. The first is the transport distance L between the user and the primary unit ($L=50\text{m}$). Next, the indoor (user's space) and outdoor air temperatures for an air-conditioning application are $T_U=25^\circ\text{C}$ and $T_O=40^\circ\text{C}$. Finally, the internal Second Law efficiency of the primary cycle is $\eta_{PC}=0.75$. This efficiency accounts for non-reversible compression and expansion, and has no reason to depend on the properties of the slurries.

The four slurries investigated herein are:

1. Slurry *IG*: Ice crystals in an aqueous solution of monopropylene-glycol (MPG) at the initial mass fraction x_0 of 0.08.
2. Slurry *CO*: Carbon-dioxide hydrate in water under CO_2 pressure P_G of 3.0MPa;
3. Slurry *TB*: Hydrate of Tetra-n-Butyl-Phosphonium Bromide (TBPB) in an aqueous solution of TBPB at the initial mass fraction x_0 of 0.20;
4. Slurry *MH*: Mixed hydrate of CO_2 -TBPB in an aqueous solution of TBPB at the initial mass fraction x_0 of 0.20 and under CO_2 pressure P_G of 0.72MPa.

Their main thermophysical characteristics are reported in Table I. Usually, ice slurries are based on more concentrated solutions, so that phase change occurs well below 0°C; this constraint is not necessary for air-conditioning applications. By its low viscosity, a low fraction x_0 is *a priori* beneficial while still presenting a case with melting temperature below 0°C. The slurries *CO* and *TB* strongly differ by their enthalpy of fusion and their viscosity; the values of P_G and x_0 were chosen in order to equate their melting temperatures and discriminate the effect of this temperature on energy efficiency. Lastly, the slurry *MH* has almost the same properties as *TB* except the melting temperature. All these choices have been made in order to compare the impacts of the various properties.

Operation of the secondary circuit, as represented in Fig. 1, depends to a large extent on the maximal and minimal crystal mass fractions X_1 at the outlet (point 1) and X_5 at the inlet (point 5) of the *HXE* heat exchanger where crystallization occurs. In order to ease crystallization in *HXE*, the slurry is assumed to always contain a small amount of crystals. This avoids nucleation delays (induction time) and subsequent supercooling, which may be significant and rather out-of-control [3]. A low but non-zero value is the given to X_5 for each slurry: 0.03. Various values of X_1 are explored in order to determine numerically the optimal operation conditions.

For given values of these two fractions, only one value of the slurry flow-rate satisfies constraint #1 on \dot{Q}_U . Constraint #4 on the Reynolds number then leads to the hydraulic diameters for the loop and the heat exchangers. Once these diameters are known, the pressure drops and heat transfer coefficients can be evaluated, leading to the refrigerant temperatures in the cooling unit. This data makes it possible to know all the fluxes mentioned in the energy balances (1) and (2), and consequently to assess the total energy consumption.

Slurry code:	<i>IG</i>	<i>CO</i>	<i>TB</i>	<i>MH</i>
T_f (°C)	-2.7	7.2	7.3	12.1
ΔH_f (kJ.kg ⁻¹)	333.5	374	204	223.5
$\mu_{\phi=0.1}$ (mPa.s)	3.7	4	7	7
$\mu_{\phi=0.2}$ (mPa.s)	5.7	9	17	17
Y_W	1	0.746	0.612	0.587
Y_A	0	0	0.368	0.342
Y_{CD}	0	0.254	0	0.071
Optimal X_1	0.20	0.16	0.14	0.14
w_T [-]	0.27	0.22	0.22	0.20
T_E [°C]	-9.5	+0.27	+0.77	+4.36

Table I: Thermophysical properties of the four slurries under consideration: fusion temperature T_f , enthalpy of fusion ΔH_f , effective dynamic viscosity with $\phi=0.1$ and $\phi=0.2$ (slurry velocity=1m.s⁻¹; tube diameter=30mm), and stoichiometry of the crystals (mass fractions Y_i of water, additive and carbon dioxide). Results of calculations in the last three lines: optimal value of X_1 , non-dimensional total energy consumption w_T , and evaporation temperature T_E .

4 Numerical model

4.1 Mass balances

Although they consist of a liquid phase containing solid crystals, usual slurries are considered as single fluids. When no gas molecule is involved in the solid phase (slurries *IG* and *TB*), the flow consists of the slurry alone and is ruled by the two-phase equilibrium between solid (ice or salt-hydrate) and liquid aqueous solution. When the solid phase involves a gas molecule (slurries *CO* and *MH*), a difference is made here-under between the *slurry*, i.e. the liquid plus solid phases alone, and the *flow* produced by the *slurry* plus the CO₂ vapor phase when present. The *flow* is then ruled by the three-phase equilibrium between solid hydrate, liquid water or salt solution (plus dissolved CO₂) and vapor, particularly in the heat exchangers where phase change occurs. The mass balances here-under are established for the most complex configuration, three components (water, additive, and carbon dioxide) in presence of gas. For the sake of stationarity, the mass fractions χ_W , χ_A , and χ_{CD} are constant and uniform (

$\chi_W + \chi_A + \chi_{CD} = 1$), where χ_A or χ_{CD} may equal zero, but not both. The phase composition of the *flow* is given by the mass fractions χ_S , χ_L , and χ_G respectively for the solid, liquid and gas phases ($\chi_S + \chi_L + \chi_G = 1$). As water and additive only exist in the solid and liquid phases, one has: $\chi_{\bullet} = \chi_{\bullet,S} + \chi_{\bullet,L}$, for $\bullet = W$ or A . When present, carbon dioxide exists in each phase, hydrate, liquid (dissolved) and gas (pure CO_2): $\chi_{CD} = \chi_{CD,S} + \chi_{CD,L} + \chi_G$.

Each crystal under consideration has its own stoichiometry written as: $\chi_{\bullet,S} = Y_{\bullet} \cdot \chi_S$, with $\bullet = W, A$ or CD and $\sum_{\bullet} Y_{\bullet} = 1$. The four sets of Y_{\bullet} are given in Table I. Once the material compositions and the solid fraction χ_S are determined, all the other mass fractions mentioned above can be deduced.

However, for the slurries with additive (*IG*, *TB* and *MH*), the equilibrium temperature T_{eq} depends on the additive concentration in its aqueous solution $x = \chi_{A,L} / (\chi_{A,L} + \chi_{W,L})$, see Fig. 2. The relationship between x , its so-called *initial* (before crystallization) value $x_0 = \chi_A / (\chi_A + \chi_W)$, and the mass fractions χ_{\bullet} , is given as:

$$x = \frac{x_0 \cdot (1 - \chi_{CD}) - Y_A \cdot \chi_S}{(1 - \chi_{CD}) - (Y_A + Y_W) \cdot \chi_S} \quad (3)$$

The crystal mass fraction in the *slurry*, X , is also a key parameter for many thermophysical properties of the *slurry* (density, heat capacity, conductivity, viscosity) described in the Appendix. It is simply given as $X = \chi_S / (\chi_L + \chi_S) = \chi_S / (\chi_A + \chi_W + \chi_{CD,L} + Y_{CD} \cdot \chi_S)$.

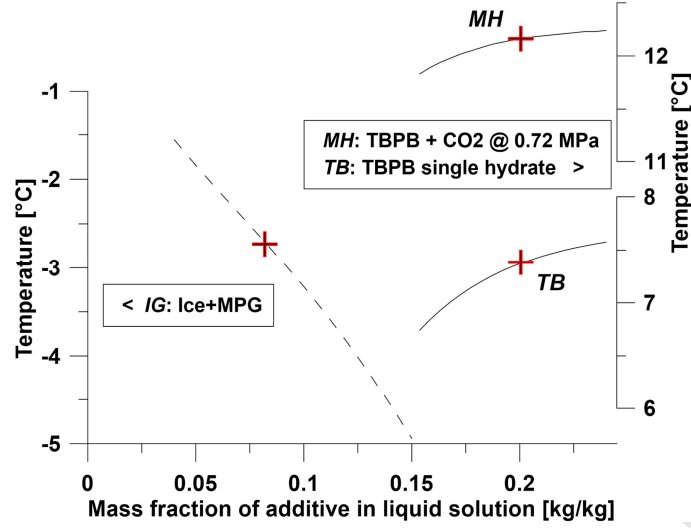


Fig. 2: Equilibrium temperature as a function of the additive concentration for the three slurries *IG*, *TB*, and *MH*. The crosses indicate the *initial* concentrations x_0 in the completely melted solutions.

Even with the slurries *CO* and *MH*, it is assumed that a gas-free *slurry* is supplied to the secondary circuit. Indeed, in real installations a storage tank is usually implemented at the outlet of the crystallizer *HXE* [23]. There, separation between gas and slurry occurs naturally due to gravity. Moreover, the gas generated by crystal fusion in *HXU* would make the slurry-gas *flow* in the return line (45) rather complex and difficult to control. The gaseous CO_2 will likely be separated from the *slurry*, e.g. in a cyclone implemented at the outlet of *HXU*. In such a case, the lines (123) and (45) are free of gas ($\chi_G = 0$ and $X = \chi_S$) while the gas returns to crystal generation in *HXE* via a separate line (67). Although finally negligible, the mechanical work required for recompressing this gas flow was considered in this study, as well as the mass balance at the separation between the lines (67) and (45):

$$\dot{m}_7 = \dot{m}_1 - \dot{m}_5 = Y_C \cdot (\dot{m}_1 \cdot X_1 - \dot{m}_5 \cdot X_5) \quad (4)$$

4.2 Enthalpy balances and heat exchanges

In addition to eq. (1), the enthalpy balances involved in the secondary loop are:

$$\dot{Q}_U = \dot{m}_5 \cdot (h_4 - h_3) + \dot{m}_7 \cdot (h_6 - h_3) \quad , \quad -\dot{Q}_E = \dot{m}_5 \cdot (h_1 - h_5) + \dot{m}_7 \cdot (h_1 - h_7) \quad (5)$$

$$\dot{m}_1 \cdot (h_3 - h_1) = 0.5 \cdot \dot{Q}_I + \dot{W}_P \quad , \quad \dot{m}_5 \cdot (h_4 - h_5) = 0.5 \cdot \dot{Q}_I \quad , \quad (6)$$

$$\dot{W}_P = (\dot{m}_1 / \rho_1) \cdot (\Delta P_{23} + \Delta P_{HXU} + \Delta P_{45} + \Delta P_{HXE}) \quad (7)$$

$$\dot{m}_7 \cdot (h_7 - h_6) = \dot{W}_G \quad \text{when relevant} \quad (8)$$

The enthalpy gain (h_7-h_6) by compression of gaseous CO₂ in the compressor *CG* at the outlet of *HXU* is based on an isentropic efficiency of 0.8. Herein, the enthalpy of the *flow* is a function of both temperature and composition, and not of pressure. First, only the gas phase is compressible, and its weight is weak. Second, the extra pressure related to pressure drops in the loop is applied to the *flow* by the pump *P* without adding any CO₂ into the liquid phase. The amount of dissolved CO₂ in the liquid phase, with which the solid phase is in equilibrium, is thus unchanged, and remains unchanged when pressure decreases along the loop. It can be inferred that the CO₂ partial pressure P_G is uniform along the circuit. After introducing the average heat capacity $\overline{c_p}$ of the *flow*, the isobaric change of enthalpy is written:

$$dh = \overline{c_p} \cdot dT - \Delta H_f \cdot d\chi_S \quad (9)$$

In each heat exchanger, *HXE* or *HXU*, the gradient of the *flow* enthalpy in steady state with negligible longitudinal conduction is ruled by:

$$\dot{m} \cdot \frac{dh}{dy} = (U\Pi)_{\bullet} \cdot (T_{\bullet} - T) \quad (10)$$

where $(U\Pi)$ is the global thermal conductance per unit length [in W.m⁻¹.K⁻¹] between either the primary refrigerant ($\bullet=E$) or the air-conditioned room ($\bullet=U$), and the *flow* in the heat exchanger. The tube diameter in each heat exchanger is determined from the total flow rate \dot{m} , the rheological properties of the slurry, and constraint #4 on the Reynolds number. The *wetted perimeters* Π_{\bullet} can then be evaluated. Equations (9) and (10) can be solved once the

relationship between dT and $d\chi_S$ is known. As phase change is assumed to occur at the equilibrium temperature $T_{eq}(x, P_G)$, two cases must be considered before global resolution.

4.2.1 Slurries with additive

For the slurries *IG*, *TB*, and *MH*, T_{eq} depends on the additive concentration x . Using the partial derivative $(\partial T_{eq}/\partial x)_{P_G}$ and the relation between x and χ_S at constant total mass (liquid+solid+gas), eq. (3), the partial derivative $(\partial T_{eq}/\partial \chi_S)_m$, denoted as β in the following, can be defined such that:

$$dT = dT_{eq} \equiv \left[\left(\frac{\partial T_{eq}}{\partial x} \right)_{P_G} \cdot \left(\frac{dx}{d\chi_S} \right)_m \right] \cdot d\chi_S = \beta \cdot d\chi_S \quad (11)$$

The enthalpy gradient can be rewritten in terms of temperature gradient:

$$\dot{m} \cdot \left(\bar{c}_p - \frac{\Delta H_f}{\beta} \right) \cdot \frac{dT}{dy} = (U\Pi)_\bullet \cdot (T_\bullet - T) \quad (12)$$

This equation is non-linear because the coefficients \bar{c}_p , β , and U depend on χ_S . Each heat exchanger is discretized into sections where eq. (12) can be linearized. Along one section, the equation of state is linearized as $T_{eq} = T_{in} + \beta \cdot (\chi_S - \chi_{Sin})$, where the index 'in' refers to the inlet of the section under consideration. The solution of the linearized equation (12) is an exponential function of the distance y from the section inlet: $T = T_{in} + \Delta T \cdot (1 - e^{-\mu y})$.

Introducing this expression into (11) and (12) leads to:

$$\chi_S = \chi_{Sin} + (\Delta T / \beta) \cdot (1 - e^{-\mu y}) \quad (13)$$

with $\Delta T = T_\bullet - T_{in}$, and $\mu = \beta \cdot (U\Pi)_\bullet / \left[\dot{m} \cdot \left(\beta \cdot \bar{c}_p - \Delta H_f \right) \right]$.

4.2.2 CO_2 single hydrate slurry

The slurry CO falls into the second case: there is no additive ($x=0$), and T_{eq} only depends on the CO_2 pressure P_G . In this case, temperature is uniform as is pressure: $T = T_{in}$, and equation (10) becomes

$$-\Delta H_f \cdot \dot{m} \cdot \frac{d\chi_S}{dy} = (U\Pi)_\bullet \cdot (T_\bullet - T_{in}) \quad (14)$$

the solution of which is:

$$\chi_S = \chi_{Sin} - \frac{(U\Pi)_\bullet \cdot (T_\bullet - T_{in})}{\dot{m} \cdot \Delta H_f} \cdot y \quad (15)$$

4.2.3 Global resolution

The values of χ_S at the inlet and outlet of each heat exchanger are prescribed. Each heat exchanger (HXU or HXE) is sub-divided into sections where the flow composition χ_S changes by given $\Delta\chi_S$ and the *flow* thermophysical properties are almost uniform. The length of each section Δy thus depends on the local rate of phase change. Global resolution is not the same for HXU and HXE . For HXU , the temperature T_U is known but not the heat exchange area. The length of HXU , L_{HXU} , is calculated as the one for which the value of χ_S at the outlet of HXU is consistent with the prescribed value of X_5 . The area A_{HXU} is then given by $A_{HXU} = L_{HXU} \cdot \Pi_U$. For HXE , the heat exchange area A_{HXE} is known, but the evaporation temperature T_E is not. The section lengths are adapted for their sum to equate A_{HXE} / Π_E , and T_E takes the value for which the value of χ_S at the outlet of HXE corresponds to the value of X_1 under consideration.

The data and formulae used for evaluating the heat transfer and friction parameters are described in the Appendix. Lastly, the rheological laws given in the Appendix result in pressure drops in the heat exchangers ΔP_{HXE} and ΔP_{HXU} .

5 System optimization, results, and discussion

5.1 Numerical results

The relations and rules described above leave two degrees of freedom in the design of the slurry loop: 1) the crystal mass fraction X_1 at the outlet of the crystal generator HXE , and 2) the tube diameter D of the slurry loop. Once X_1 and D are given, the only value of \dot{m} that satisfies the equations (5) to (8) is calculated iteratively. This calculation simultaneously gives the heat exchanger parameters (tube diameter and length), and thus the values of ΔP_{23} , ΔP_{45} , ΔP_{HXE} , ΔP_{HXU} , \dot{W}_P , \dot{Q}_I , \dot{W}_G , \dot{Q}_E . A third short iteration solves the values of T_C , COP , and \dot{W}_{PC} , which results in the total electric consumption \dot{W}_T .

Two figures of merit related to energy efficiency arise from the derivation above: 1) the pumping power for the secondary loop ($\dot{W}_P + \dot{W}_G$) and 2) the total mechanical (electrical) power \dot{W}_T , which is the quantity minimized by the optimization procedure. For the sake of generality, they are made non-dimensional according to: $w_P = (\dot{W}_P + \dot{W}_G) / \dot{Q}_U$ and $w_T = \dot{W}_T / \dot{Q}_U$. As the pumping power w_P is an auxiliary cost on the order of 10^{-2} , the total power consumption w_T is mainly due to the primary compressor and thus lies slightly above $1/COP$. Those two figures of merit are complemented by the total pressure drop and by the Reynolds number in the loop line (123), where the risk of crystal deposition is the highest. The results for slurries *IG* (ice-glycol) and *MH* (mixed hydrate) are given in Figures 3 and 4 respectively; they exhibit similar trends. The results for the slurries *CO* and *TB*, which are very similar, are not displayed herein.

Those figures first show the extent to which the optimization criterion is crucial. If the analysis solely considered the secondary loop, then the configurations denoted as ‘A’ in those figures would seem optimal: the pumping power and the pressure drop are both minimal with a strongly turbulent flow ($Re > 4000$). The selected mass fraction X_1 would be low (0.10-0.12, and probably less if such range had been investigated). The present global approach leads to quite different optimal values, as shown by points ‘B’: the optimal value of X_1 now

lies around 0.20 for the *IG* slurry, and around 0.14 for *MH*. Meanwhile, from points ‘A’ to points ‘B’, the total electrical consumption is reduced by 12-15%, which is not insignificant.

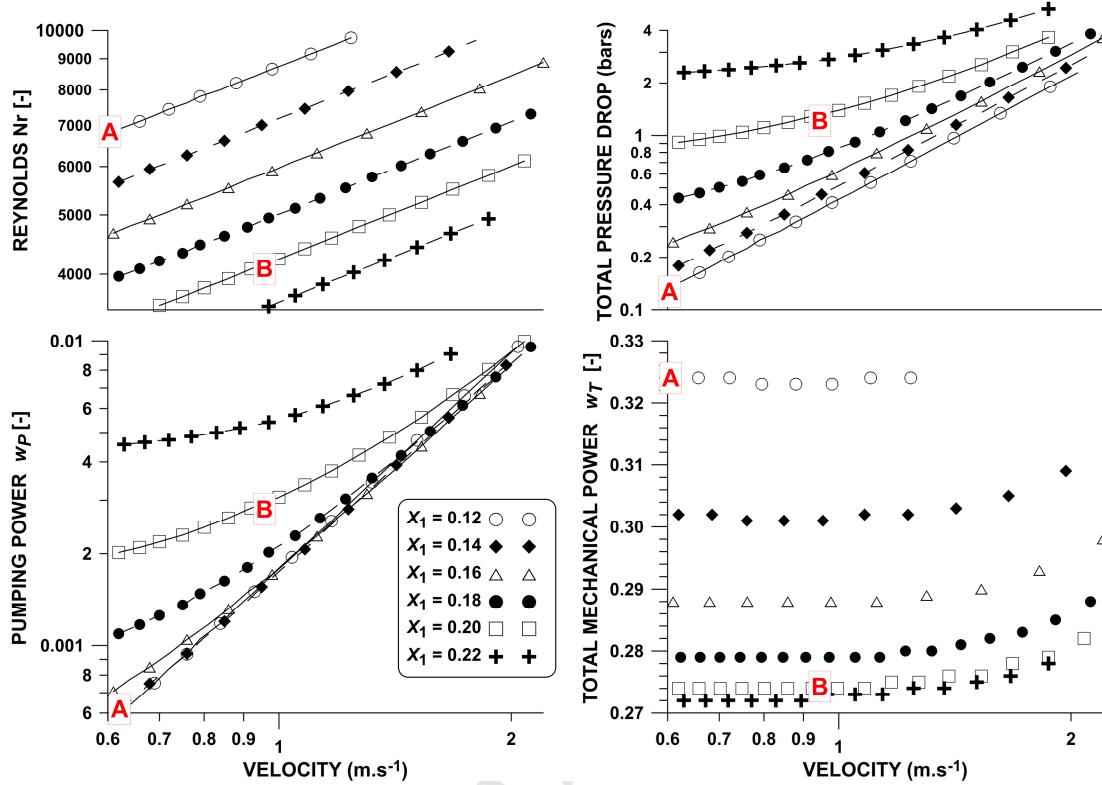


Fig. 3: Flow conditions (velocity, Reynolds number in the line 23, total pressure drop) and energy consumption (pumping power and total) calculated with the slurry *IG* (ice-glycol) for various values of the mass fraction X_1 and loop tube diameter D . The configuration described by Point A would be declared optimal when considering the secondary loop alone (lowest pumping power w_p), while that described by Point B emerges as globally optimal (lowest total mechanical power w_T).

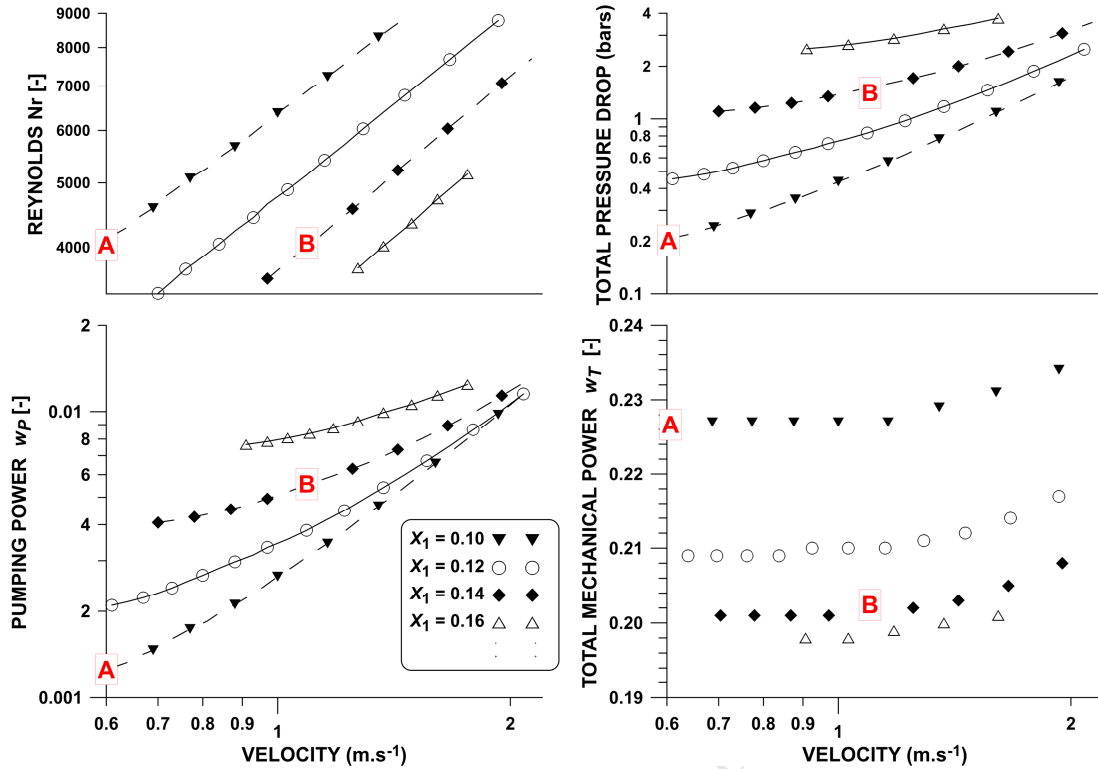


Fig. 4: Flow conditions calculated with the slurry *MH* (CO₂-TBPB mixed hydrate). Same legend as for Fig. 3.

5.2 Existence of an optimal value of X_1

This section analyzes the effects of the upper bound of the solid fraction X_1 . The following text only considers *increases in X_1* in order to avoid tedious repetitions. Readers are thus asked to complete incomplete-looking phrases with ‘...when X_1 increases’. Numerical examples are calculated for the slurry *IG*: the notation [$\bullet_1 \rightarrow \bullet_2$] means that the specified quantity changes from \bullet_1 to \bullet_2 when X_1 increases from 0.12 to 0.22.

The slurry mainly transports latent heat, the cooling power \dot{Q}_U may thus be approximated by $\dot{m} \cdot (X_1 - X_5) \cdot \Delta H_f$, where $X_5 = 0.03$. When X_1 increases from 0.12 to 0.22, $\Delta X = X_1 - X_5$ is multiplied by a factor slightly above 2. If X_1 were changed alone without changing anything

else in the process design, then the fluxes \dot{Q}_U , \dot{Q}_E , and \dot{Q}_C would approximately double while keeping the same heat exchange areas. A same design of the process cannot correctly fit to such a range of power rates, and such an approach forcedly leads to the smallest possible X_1 as optimal, just because it trivially minimizes the rate of irreversibility. The present approach differs completely and leads to quite different conclusions.

5.2.1 Mass and heat transport phenomena

In order to keep \dot{Q}_U constant when X_1 increases (constraint #1), the slurry flow rate \dot{m} must be reduced [1.0- \rightarrow 0.47kg.s⁻¹]. Moreover, the increase in X_1 also modifies the properties of the *flow* in the heat exchangers: the viscosity of the slurry noticeably increases with the crystal mass fraction, as described in the Appendix. In order to fulfill the constraint #4 on the Reynolds number, the tube diameter D and the *flow* velocity u in the heat exchangers must follow significant changes: [80- \rightarrow 22mm] and [0.2- \rightarrow 1.25m.s⁻¹], respectively. Integration of the local pressure gradient ($dP/dy = -2f \cdot \rho \cdot u^2 / D$) over the length of each heat exchanger leads to the respective pressure drop ΔP_{HX} . The formulae giving the local Fanning factor f as functions of D , u and X are reported in the Appendix. Due to the slightly different constraint on the Reynolds number, ΔP_{HXE} is larger than ΔP_{HXU} . In addition, the heat exchange area A_{HXE} is prescribed (constraint #2), the tube length in the *HXE* also changes like $1/D$, so that ΔP_{HXE} finally is a quasi-exponential function of X_1 , with an increases close to three orders of magnitude [0.5- \rightarrow 200kPa], see Figure 5.

Besides, the local heat transfer coefficient between the slurry and the heat-exchanger tube also depends on D , u , and X (see the Appendix). After addition of the heat transfer resistance between tube and refrigerant and resolution of the temperature field for the slurry (see section 4.2), one obtains the average temperature difference between slurry and refrigerant along

HXE , $\overline{\Delta T_E} = \overline{T_f - T_E}$. Figure 5 shows that $\overline{\Delta T_E}$ significantly decreases over the investigated range [14.6->6.1K], and that the curve admits a lower asymptotic bound, close to 3.3K in the present case (the total heat transfer resistance between the slurry and the refrigerant does not vanish).

5.2.2 Minimization of total energy consumption: an optimal value of X_1

The total energy consumption w_T sums up that of the primary compressor, w_{PC} , plus that of the two circulation pumps, $w_P + w_G$. When present, w_G is very weak and scarcely depends on X_1 : only w_P and w_{PC} are important in the analysis. The pumping power w_P [$= \Delta P_T \cdot \dot{m} / (\rho_1 \cdot \dot{Q}_U)$], curve with black + in Figure 5, increases very significantly [6×10^{-5} -> 660×10^{-5}], with a much stronger slope for the large values of X_1 . The consumption of the primary compressor is given by:

$$w_{PC} = \frac{1 + w_P + w_G}{\eta_{PC}} \cdot \left(\frac{T_C - T_E}{T_E} \right) \quad (16)$$

Figure 5 shows that w_{PC} depends on X_1 with the same trend as $\overline{\Delta T_E}$ (solid curve bottom). All those results show that there exists an optimal value of X_1 . When X_1 increases in the low range [0.12 - 0.14], the pumping power w_P is so low compared to w_{PC} (6×10^{-5} vs. 0.33) that even a factor of 3 leaves it negligible in the total balance. Meanwhile, the substantial increase in the evaporation temperature (+3.3K) significantly reduces the difference ($T_C - T_E$), and therefore the power rate w_{PC} . When X_1 lies in the high range [0.20 - 0.22], the pumping power w_P has become significant (2.8×10^{-3}) and the evaporation temperature gets closer to its asymptotic limit. With the same increase in X_1 , w_P increases by a factor of 2.3, i.e. by $+3.8 \times 10^{-3}$, and T_E increases by (+0.7K) only, so that the resulting decrease in w_{PC} is of (6×10^{-3}) only. This development shows that there is a trade-off between the increasing power

consumed by the circulation pumps and the decreasing power consumed by the primary compressor. This trade-off could not be evidenced if the analysis were limited to the secondary loop only.

The existence of an energetically optimal value of X_1 is an argument supporting the efficiency of two-phase fluids for the purpose of secondary refrigeration compared to single-phase fluids.

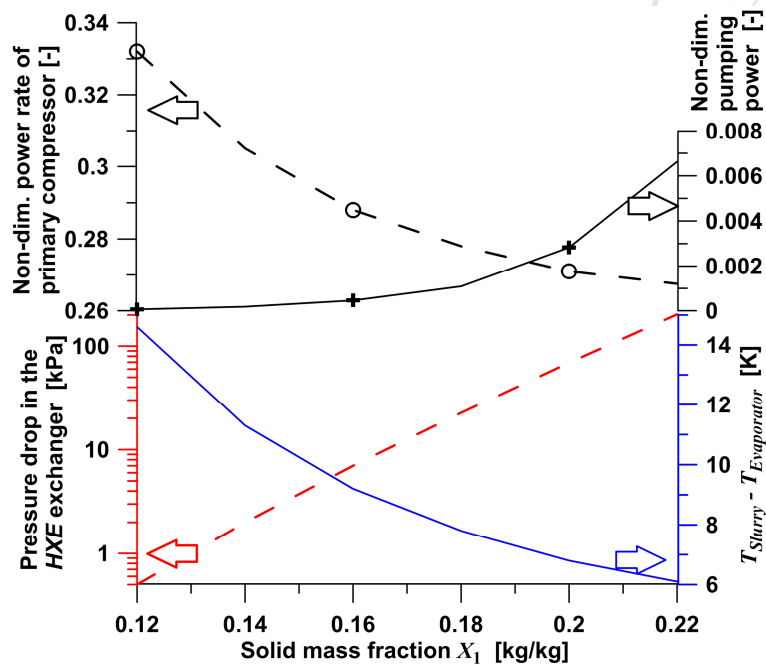


Fig. 5: Bottom: thermo-hydraulic data in the *HXE* heat exchanger calculated with the *IG* slurry as functions of the mass fraction X_1 . Dashed red line: pressure drop ΔP_{HXE} ; solid blue line: average temperature difference $\overline{\Delta T_E}$ between slurry and evaporation.

Top: Components of the non-dimensional total energy consumption. Dashed line with circles: power of primary compressor w_{PC} ; solid line with crosses: pumping power w_P .

5.3 Fusion temperature is the main parameter for energy performance

A comparison of Figs. 3 and 4 shows that using the slurry *MH* rather than *IG* reduces total energy consumption w_T by 25%. Although both enthalpy of fusion and viscosity adversely

impact MH (see Table I), the pumping power can be maintained at an auxiliary level via an adapted circuit design. In parallel with the 15K increase in fusion temperature, the evaporation temperature rises from -9.5 (IG) to $+4.4^\circ\text{C}$ (MH), i.e. an increase of $+14\text{K}$. With $T_C=46^\circ\text{C}$, the difference $(T_C - T_E)$ is thus decreased by 25%, and the total energy consumption decreases by the same proportion.

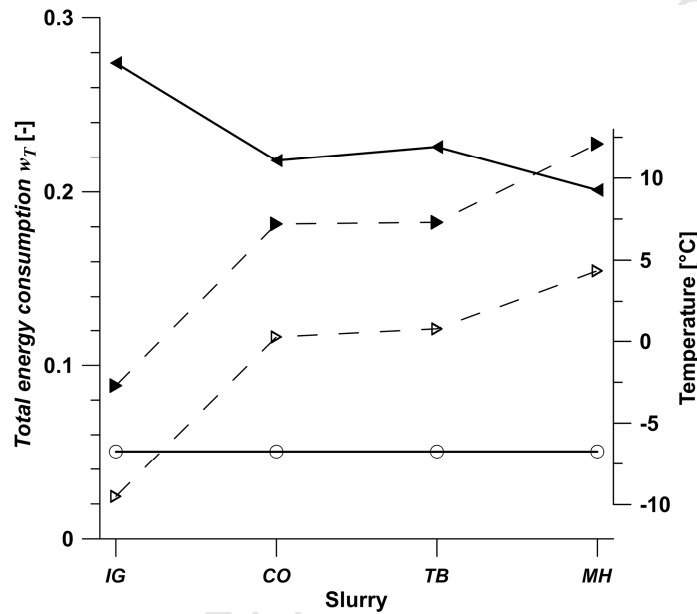


Fig. 6: Calculated total power consumption w_T for each slurry (symbol ◀) compared to that of the reversible process (symbol ○). The dashed lines show the fusion and evaporation temperatures (respectively ▶ and ▷).

Two other slurries were considered in this study, TB and CO . They have the same fusion temperature, but with respect to latent heat of fusion and viscosity, CO is closer to IG and TB closer to MH . They also exhibit an optimal value of X_1 given in Table I. Figure 6 compares, the global performance obtained for each of the four slurries, after having optimized the system individually as described above. If the process were reversible, the non-dimensional energy consumption would be the same for all slurries (solid line with open circles). The calculated values of w_T (solid line with closed triangles) clearly exhibit three levels (within

accuracy of calculations), closely reproducing the three values of fusion temperature (see Table I). It can thus be concluded that, among the characteristics under consideration herein, the temperature of fusion is what governs the energy efficiency of a secondary refrigeration process, while changes in enthalpy of fusion and viscosity can be compensated for by adapting the design of the circuit and heat exchangers.

6 Comparison with experimental data

The literature reporting experimental data measured on secondary refrigeration systems of industrial size is more than rare. Most of the experimental data published are obtained from lab-size setups. One of the largest experiment reported is that of Shi and Zhang [24]. They produce 185kg of tetra-n-butyl-ammonium-bromide clathrate hydrate (which is rather similar to TBPB) in a double-tube heat exchanger cooled by a refrigerator. The hydrate slurry is stored in a 0.314m^3 large vessel. The slurry is then melted in a plate heat exchanger. There are many differences between the two studies: cyclic crystallization/melting vs. steady-state, at least one order of magnitude regarding power rates, one setup tested with various maximal values of X vs. optimal design according to the maximal value of X , but some features are not in contradiction. First, depending on the crystallization method, they obtain their best performance for crystallization up to $X=0.10$ (*homogeneous crystallization*) and $X=0.20$ (*heterogeneous crystallization*), when our optimal value of X_1 with TBPB is 0.14. Second, those authors obtained values of COP around 2.6 when we claim for 4.3. However, their refrigerator only supplies 2-3kW cooling, when our calculations considered a cooling power of 30kW. Larger refrigerators are more efficient. Third, the difference in cooling rates must also be considered when comparing the pressure drops: 10 to 15kPa in their double-tube heat exchanger and 70-100kPa in our HXE. Our calculations are not in contradiction with their experimental data.

7 Conclusion

A global approach following the principles of optimization (minimization of an objective function under explicit given constraints) was applied to the process of secondary refrigeration in order to compare various hydrate slurries in terms of global efficiency. Analysis shows, that for given heat-exchange areas, there exist optimal operating conditions, which are specific for each slurry. Analysis also shows that among all their thermophysical characteristics, the crystal melting temperature is the leading parameter for global performance of the process.

The difference between the calculated values of energy consumption and the one given by a reversible process is interpreted in terms of exergy losses in Part 2 of this article [Pons et al., *Energy, present issue*]. The effects of phase change kinetics are also investigated. Further perspectives include modelling transient behaviors in secondary refrigeration loops.

Acknowledgement

This work was financed by the French National Agency for Research (ANR) [project *CRISALHYD* # ANR-14-CE05-0045].

Appendix: Thermophysical properties

This appendix does not intend to review the state-of-the art on the thermophysical properties of the four slurries under consideration, but rather to provide the values or simplified correlations that were used in the calculations.

A.1 Equations of state

The equations of state $T_{eq}(x)$ for the slurries *IG*, *TB*, and *MH*, as established from initial data of [25-28], are shown in Fig. 2 and the values used herein are given in Table I.

For the slurry CO , the equilibrium temperature T_{eq} depends on the gas pressure only. The data of [29-31] are linearized in the range of interest according to: $\ln(P) = 0.098 + 0.139 \cdot T$, with T in Celsius and P in MPa.

For the solubility σ of CO_2 in the water- CO_2 solution, a model was adjusted to the data published in [32] leading to the following formula (mass concentration):

$$\sigma(T, P_G) = \frac{\chi_{CD,L}}{\chi_{CD,L} + \chi_{W,L}} = \frac{A \cdot P_G^2 + B \cdot P_G}{1 + 0.5907 \cdot (A \cdot P_G^2 + B \cdot P_G - 1)} \quad (A.1)$$

where $A = (-126 + 5 \cdot T) \times 10^{-5}$, and $B = (138 - 4 \cdot T) \times 10^{-4}$, with T in Celsius and P_G in MPa.

A.2 Density

The *flow* density is obtained by summing up the volumes of each phase: $\rho^{-1} = \sum_{\bullet} \chi_{\bullet} \cdot \rho_{\bullet}^{-1}$, with $\bullet = S, L$, and G . For one slurry, temperature is fixed by the solid-liquid equilibrium, so that ρ_S and ρ_L are either constant or x -dependent, see Table A.I [33]. Density of gaseous CO_2 (a non-ideal gas) is given by $\rho_G = P / (Z \cdot r \cdot T)$, with $Z = 0.997 - 0.298 \cdot T_r \cdot P_r - 0.344 \cdot (T_r \cdot P_r)^2$, where T_r and P_r are the reduced temperature and pressure, respectively.

A.3 Heat capacity

The *flow* average heat capacity is: $\overline{c_p} = \sum_{\bullet} \chi_{\bullet} \cdot c_{p\bullet}$. The various heat capacities, constant or x -dependent, are taken from [28, 33-35] and given in Table A.I. The values of c_{pS} for hydrates involving TBPB were replaced by those with TBAB, which has a similar hydration number and which has been more widely investigated. The difference is likely to be negligible compared to the role of enthalpy of fusion. The values of c_{pG} (gaseous CO_2) are deduced from [36].

Slurry Code:	<i>IG</i>	<i>CO</i>	<i>TB</i>	<i>MH</i>
ρ_S [kg.m ⁻³]	917	1066	1145	1233
ρ_L [kg.m ⁻³]	$1002 + 85.2 \cdot x$	1000	$1000 + 80 \cdot x$	
c_{pS} [J.kg ⁻¹ .K ⁻¹]	2050	2085	2560	2685
c_{pL} [J.kg ⁻¹ .K ⁻¹]	$4258 - 1070 \cdot x$	4198	$4180 - 1568 \cdot x$	
c_{pG} [J.kg ⁻¹ .K ⁻¹]	-	902	-	848
$1000 \cdot K$	$2.4 \cdot \exp(4.36 \cdot \phi)$ [Pa.s]	$1.8 \cdot \exp(18 \cdot \phi)$	$7.4 \cdot \exp[13 \cdot \phi \cdot (1 - 1.3 \cdot \phi)]$	
n	1	$1 - 1.8 \cdot \phi$	$0.98 \cdot \exp[-3.59 \cdot \phi \cdot (1 - 1.3 \cdot \phi)]$	
k_S [W.m ⁻¹ .K ⁻¹]	2.2	2.2	0.42	0.42
k_L [W.m ⁻¹ .K ⁻¹]	0.55	0.55	0.49	0.49

Table A.I: Material properties used in the calculations (x is the mass concentration of additive in the aqueous solution).

A.4 Viscous friction and heat transfer

These two phenomena depend much more on the solid volume fraction ϕ in the *slurry* than on the mass fraction X . The expression of ϕ is given by simple algebra: $\phi = \rho_L \cdot X / [\rho_L \cdot X + \rho_S \cdot (1 - X)]$. Moreover, most *slurries* are non-Newtonian fluids where the shear stress τ depends on the shear rate $\dot{\gamma}$ according to the *Ostwald-de Waele (OdW)* law: $\tau = K \cdot \dot{\gamma}^n$. Although the question is still open, the ice slurry *IG* with low crystal fraction can be seen as Newtonian ($n=1$, and with K as the dynamic viscosity) [37], when the three other slurries *CO*, *TB*, and *MH*, are pseudo-plastic fluids ($n < 1$). The values of K and n used herein were obtained from [12, 38-40], and simplified formulae are given in Table A.I. For *OdW* fluids, the Reynolds number is given by the Metzner-Reed formula [41]:

$$Re = \frac{u^{2-n} \cdot D^n \cdot \rho}{K} \cdot 8 \cdot \left(\frac{n}{6n+2} \right)^n \quad (\text{A.2})$$

where u is the *slurry* velocity and D the tube diameter. For laminar flows, the Fanning friction factor f is given by the same formula as for Newtonian fluids ($f = 16/Re$), but the relation for turbulent flows is:

$$\frac{1}{\sqrt{f}} = \frac{4}{n^{0.75}} \cdot \log_{10} \left(Re \cdot f^{1-n/2} \right) - \frac{0.4}{n^{1.2}}$$

Transition from laminar to turbulent flow takes place for $2000 < Re < 4000$. Therefore, flows are considered herein as fully turbulent, and thus preventing crystal deposition, for $Re=4000$.

As turbulence is imposed everywhere, the latter formula on f gives way to the four pressure drops ΔP_{23} , ΔP_{HXU} , ΔP_{45} , ΔP_{HXE} , from which the pumping power is evaluated by eq. (7).

Studies about heat transfer in non-Newtonian slurries are scarce, with the exception of the review [42]. Following the latter reference, we used the empirical formula:

$$Nu_{SL} = \left(0.023 \cdot Re^{0.8} \cdot Pr^{0.4} \right) \cdot \left[1 + 0.076 \cdot (\exp(\phi) - 1) - 647 \cdot 10^{-7} \cdot \phi^{0.562} \cdot Re^{0.827} \right] \quad (A.3)$$

complemented by the expression given by [43] for the *slurry* thermal conductivity k_{SL} :

$$k_{SL} = k_L \cdot \left[1 + \phi \cdot \varepsilon \cdot (1 + \phi \cdot \varepsilon \cdot (0.33 + 0.04 \cdot \varepsilon)) \right], \text{ where } \varepsilon = (k_S - k_L) / [(1 - (k_S - k_L)) / 3].$$

The values of k_S and k_L given in Table A.I are extracted from [33, 42].

Bibliography

- [1] Bellas I, Tassou SA. Present and future applications of ice slurries. *Int J Refrig-Rev Int Froid*. 2005;28(1):115-21.
- [2] Cowan D, Gartshore J, Chaer I, Francis C, Maidment G. REAL Zero – Reducing refrigerant emissions & leakage - feedback from the IOR Project Proc Inst R 2009-10: IOR The Institute Of Refrigeration; 2010. p. 16.
- [3] Sloan ED, Koh CA. *Clathrate Hydrates of Natural Gases Third Edition Preface*. 3rd ed. Boca Raton, FL: CRC Press-Taylor & Francis Group, 2008.
- [4] Zhang P, Ma ZW. An overview of fundamental studies and applications of phase change material slurries to secondary loop refrigeration and air conditioning systems. *Renew Sust Energ Rev*. 2012;16(7):5021-58.
- [5] Mota-Babiloni A, Navarro-Esbri J, Barragan-Cervera A, Moles F, Peris B, Verdu G. Commercial refrigeration - An overview of current status. *Int J Refrig-Rev Int Froid*. 2015;57:186-96.
- [6] Oignet J, Delahaye A, Torre JP, Dicharry C, Hoarng HM, Clain P, et al. Rheological study of CO₂ hydrate slurry in the presence of Sodium Dodecyl Sulfate in a secondary refrigeration loop. *Chem. Engng. Sci.*. 2017;158:294-303.
- [7] Wang ZB, Li FX, Fan TT, Xiong W, Yang B. Research on the Application of Gas Hydrate in Cool Storage Air Conditioning. In: Sun Y, Pei J, editors. 9th Int. Symposium on Heating, Ventilation and Air Conditioning. Amsterdam: Elsevier Science Bv; 2015. p. 1118-25.
- [8] Ogoshi H, Takao S. Air-conditioning system using clathrate hydrate slurry. JFE TECHNICAL REPORT: JFE; 2004. p. 1-5.
- [9] Youssef Z, Delahaye A, Huang L, Trinquet F, Fournaison L, Pollerberg C, et al. State of the art on phase change material slurries. *Energy Conversion and Management*. 2013;65:120-32.
- [10] Sharma V, Fricke B, Bansal P. Comparative analysis of various CO₂ configurations in supermarket refrigeration systems. *Int J Refrig-Rev Int Froid*. 2014;46:86-99.
- [11] Mahmoudi B, Naeiji P, Varaminian F. Study of tetra-n-butylammonium bromide and tetrahydrofuran hydrate formation kinetics as a cold storage material for air conditioning system. *J Mol Liq*. 2016;214:96-100.
- [12] Jerbi S, Delahaye A, Oignet J, Fournaison L, Haberschill P. Rheological properties of CO₂ hydrate slurry produced in a stirred tank reactor and a secondary refrigeration loop. *Int J Refrig*. 2013;36(4):1294-301.
- [13] Zhang P, Ma ZW, Bai ZY, Ye J. Rheological and energy transport characteristics of a phase change material slurry. *Energy*. 2016;106:63-72.
- [14] Zhang P, Ma Z, Nie D. Experimental Investigation of Flow and Heat Transfer Characteristics in the Generation of Clathrate Hydrate Slurry. *Heat Transf Eng*. 2014;35(6-8):693-702.
- [15] Oignet J, Hoang HM, Osswald V, Delahaye A, Fournaison L, Haberschill P. Experimental study of convective heat transfer coefficients of CO₂ hydrate slurries in a secondary refrigeration loop. *Appl. Therm. Engng.*. 2017;118:630-7.
- [16] Liu WG, Wang SR, Yang MJ, Song YC, Wang SL, Zhao JF. Investigation of the induction time for THF hydrate formation in porous media. *J Nat Gas Sci Eng*. 2015;24:357-64.

- [17] Aman ZM, Akhflash M, Johns ML, May EF. Methane Hydrate Bed Formation in a Visual Autoclave: Cold Restart and Reynolds Number Dependence. *J. Chem. Engng. Data.* 2015;60(2):409-17.
- [18] Guilpart J, Stamatiou E, Delahaye A, Fournaison L. Comparison of the performance of different ice slurry types depending on the application temperature. *Int J Refrig-Rev Int Froid.* 2006;29(5):781-8.
- [19] Douzet J, Kwaterski M, Lallemand A, Chauuy F, Flick D, Herri JM. Prototyping of a real size air-conditioning system using a tetra-n-butylammonium bromide semiclathrate hydrate slurry as secondary two-phase refrigerant - Experimental investigations and modelling. *Int J Refrig-Rev Int Froid.* 2013;36(6):1616-31.
- [20] Zhou H, de Sera IEE, Ferreira CAI. Modelling and experimental validation of a fluidized bed based CO₂ hydrate cold storage system. *Applied Energy.* 2015;158:433-45.
- [21] Dufour T, Oignet J, Hoang HM, Leducq D, Delahaye A, Fournaison L, et al. Impact of pressure on the dynamic behavior of CO₂ hydrate slurry during storage process. In: Kauffeld M, editor. 11th IIR Conf. on Phase Change Materials and Slurries for Refrigeration and Air Conditioning. Karlsruhe, Germany: Int. Institute of Refrigeration; 2016. p. 189-97.
- [22] Perry RH, Green DW. *Perry's Chemical Engineers' Handbook*, 8th Edition. 8th ed: McGraw-Hill, 2007.
- [23] Compingt A, Blanc P, Quidort A. Slurry for refrigeration industrial kitchen application. In: Kauffeld M, editor. 8th IIR Conf. on Phase Change Materials and Slurries for Refrigeration and Air Conditioning. Karlsruhe, Germany: Int. Inst. Refrigeration IIR-IIF; 2009. p. 135-44.
- [24] Shi XJ, Zhang P. Cold storage by tetra-n-butyl ammonium bromide clathrate hydrate slurry generated with different storage approaches at 40 wt% initial aqueous solution concentration. *Int J Refrig-Rev Int Froid.* 2014;42:77-89.
- [25] Weast RC. *Handbook of Chemistry and Physics*. 68th ed: CRC Press (Taylor & Francis), 1987.
- [26] Bel O, Lallemand A. Study of a two phase secondary refrigerant 1: Intrinsic thermophysical properties of an ice slurry. *Int J Refrig.* 1999;22(3):164-74.
- [27] Dyadin YA, Udachin KA. Clathrate polyhydrates of peralkylonium salts and their analogs. *J Struct Chem.* 1987;28(3):394-432.
- [28] Mayoufi N, Dalmazzone D, Delahaye A, Clain P, Fournaison L, Fuerst W. Experimental Data on Phase Behavior of Simple Tetrabutylphosphonium Bromide (TBPB) and Mixed CO₂ + TBPB Semiclathrate Hydrates. *J. Chem. Engng. Data.* 2011;56(6):2987-93.
- [29] Yang SO, Yang IM, Kim YS, Lee CS. Measurement and prediction of phase equilibria for water plus CO₂ in hydrate forming conditions. *Fluid Phase Equilibria.* 2000;175(1-2):75-89.
- [30] Guilpart J, Stamatiou E, Fournaison L. The control of ice slurry systems: an overview. *Int J Refrig-Rev Int Froid.* 2005;28(1):98-107.
- [31] Jerbi S, Delahaye A, Fournaison L, Haberschill P. Characterization of CO₂ hydrate formation and dissociation kinetics in a flow loop. *Int J Refrig-Rev Int Froid.* 2010;33(8):1625-31.
- [32] Diamond LW, Akinfiyev NN. Solubility of CO₂ in water from -1.5 to 100 degrees C and from 0.1 to 100 MPa: evaluation of literature data and thermodynamic modelling. *Fluid Phase Equilibria.* 2003;208(1-2):265-90.

- [33] Clain P. Couplage entre le stockage et distribution de froid par coulis d'hydrates. Paris: Univ. Pierre et Marie Curie, 2014.
- [34] Jager A, Vins V, Gernert J, Span R, Hruby J. Phase equilibria with hydrate formation in H₂O + CO₂ mixtures modeled with reference equations of state. *Fluid Phase Equilibria*. 2013;338:100-13.
- [35] Lin W, Dalmazzone D, Fuerst W, Delahaye A, Fournaison L, Clain P. Thermodynamic properties of semiclathrate hydrates formed from the TBAB plus TBPB plus water and CO₂ + TBAB + TBPB plus water systems. *Fluid Phase Equilibria*. 2014;372:63-8.
- [36] IIF-IIR. R744 CO₂ dioxyde de carbone : Propriétés thermophysiques. Paris: IIF-IIR, 2003.
- [37] Mika L. Rheological behaviour of low fraction ice slurry in pipes and pressure loss in pipe sudden contractions and expansions. *Int J Refrig-Rev Int Froid*. 2012;35(6):1697-708.
- [38] Delahaye A, Fournaison L, Marinhas S, Martinez MC. Rheological study of CO₂ hydrate slurry in a dynamic loop applied to secondary refrigeration. *Chem. Engng. Sci.*. 2008;63(13):3551-9.
- [39] Delahaye A, Fournaison L, Jerbi S, Mayoufi N. Rheological Properties of CO₂ Hydrate Slurry Flow in the Presence of Additives. *Ind Eng Chem Res*. 2011;50(13):8344-53.
- [40] Clain P, Delahaye A, Fournaison L, Mayoufi N, Dalmazzone D, Furst W. Rheological Properties of tetra-n-butylphosphonium bromide hydrate slurry flow. *Chemical Engineering Journal*. 2012;193:112-22.
- [41] Metzner AB, Reed JC. Flow of non-newtonian fluids—correlation of the laminar, transition, and turbulent-flow regions. *AIChE Journal*. 1955;1(4):434-40.
- [42] Egolf PW, Kitanovski A, Ata-Caesar D, Stamatiou E, Kawaji M, Bedecarrats JP, et al. Thermodynamics and heat transfer of ice slurries. *Int J Refrig-Rev Int Froid*. 2005;28(1):51-9.
- [43] Jeffrey DJ. Conduction through a random suspension of spheres. *Proc R Soc Lond A-Math Phys Sci*. 1973;335(1602):355-67.

Highlights

- Global optimization must be conducted with explicit constraints
- Energy efficiency can be optimized only globally, i.e. including the primary cycle
- The process design is optimized independently for each slurry
- Each slurry presents an optimum for the maximal solid mass fraction in the process
- Energy efficiency mainly depends on melting temperature